1994ApJ...428..638S

THE ASTROPHYSICAL JOURNAL, 428:638–646, 1994 June 20
© 1994. The American Astronomical Society. All rights reserved. Printed in U.S.A.

LARGE-SCALE CHARACTERISTICS OF INTERSTELLAR DUST FROM *COBE*[1] DIRBE OBSERVATIONS

T. J. SODROSKI,[2] C. BENNETT,[3] N. BOGGESS,[3] E. DWEK,[3] B. A. FRANZ,[2] M. G. HAUSER,[4]
T. KELSALL,[3] S. H. MOSELEY,[3] N. ODEGARD,[5] R. F. SILVERBERG,[3] AND J. L. WEILAND[5]
Received 1993 August 11; accepted 1993 December 29

ABSTRACT

Observations from the *COBE* Diffuse Infrared Background Experiment of the 140 and 240 μm emission from the Galactic plane region ($|b| < 10°$) are combined with radio surveys that trace the molecular (H_2), neutral atomic (H I), and extended low-density ($n_e \sim 10$–100 cm^{-3}) ionized (H II) gas phases of the interstellar medium to derive physical conditions such as the dust temperature, dust-to-gas mass ratio, and far-infrared emissivity (1) averaged over these gas phases along each line of sight and (2) within each of these three gas phases. This analysis shows large-scale longitudinal and latitudinal gradients in the dust temperature and a decrease in dust temperature with increasing Galactocentric distance. The derived dust temperatures are significantly different from those derived in similar analyses using the *Infrared Astronomical Satellite* (*IRAS*) 60 and 100 μm data, suggesting that small (5 Å $\lesssim$ radius $\lesssim$ 200 Å) transiently heated dust particles contribute significantly to the Galactic 60 μm emission. It is found that 60%–75% of the far-infrared luminosity arises from cold ($\sim$17–22 K) dust associated with diffuse H I clouds, 15%–30% from cold ($\sim$19 K) dust associated with molecular gas, and less than 10% from warm ($\sim$29 K) dust in extended low-density H II regions, consistent with the results of the *IRAS* analyses of the Galactic 60 and 100 μm emission. Within 2° of longitude of the Galactic center, the derived gas-to-dust mass ratio along the line of sight, G_d, reverses its general trend of decreasing G_d toward the inner Galaxy and increases by a factor of $\sim$2–3 toward the Galactic center. One possible explanation for this result is that the ratio of H_2 column density to ^{12}CO intensity is lower in the Galactic center region than in the Galactic disk.

Subject headings: dust, extinction — infrared: ISM: continuum — ISM: molecules

1. INTRODUCTION

The Galactic large-scale far-infrared (FIR) emission, originally observed by Hoffmann & Frederick (1969) and later with many balloon-borne instruments (Hauser et al. 1984, and references therein), arises primarily from radiatively heated dust. The details concerning the physical properties of the dust and the nature of the stellar populations that heat it within each of the gas phases of the interstellar medium (ISM) are still a subject of intense study (see review by Cox & Mezger 1989). A major advance in the field was made possible by the successful mission of the *Infrared Astronomical Satellite* (*IRAS;* Neugebauer et al. 1984), which provided complete coverage of the sky at wavelengths of 12, 25, 60, and 100 μm with a much greater sensitivity than the earlier balloon experiments. As a result, several independent *IRAS* studies of the Galactic large-scale 60 and 100 μm emission (Sodroski et al. 1986, 1987, 1989; Bloemen, Deul, & Thaddeus 1990; and references therein) have placed important constraints on the physical conditions within the molecular (H_2), neutral atomic (H I), and extended low-density ionized (H II) gas phases of the ISM, and on the distribution of FIR luminosity among these gas phase components.

However, major issues are still unresolved, such as the nature of the stellar populations that heat the dust associated with the Galaxy's molecular gas, the equilibrium temperatures of large dust grains, the contribution of stochastically heated dust to the FIR emission (Draine & Anderson 1985; Désert, Boulanger, & Puget 1990), the dust-to-gas mass ratios within the gas phases of the ISM, and the abundance of very cold dust (Wright et al. 1991; Wright 1993). The primary reason for this situation is that *IRAS*, with its limited spectral coverage, was not sensitive to very cold dust that may constitute a significant fraction of the total dust mass in the ISM. Furthermore, small stochastically heated dust grains contribute significantly to the 60 μm *IRAS* band (Sodroski et al. 1987, 1989, hereafter Paper I and Paper II, respectively) so that dust temperatures derived from the 60-to-100 μm flux ratios tend to be larger than their equilibrium value, which also results in underestimates of dust column density.

The Diffuse Infrared Background Experiment (DIRBE) instrument on board NASA's *COBE* satellite has surveyed the entire sky in 10 photometric bands covering the wavelength region from 1 to 240 μm at an angular resolution of 0°.7. This extensive spectral coverage is able to effectively sample dust emission over a wide range of temperatures. In this paper, our analysis is restricted to the 140 and 240 μm observations, since the shorter wavelength (i.e., 60 and 100 μm) detectors are believed to have a nonlinear responsivity that will be characterized in future analyses. The modeling approaches of Paper I and Paper II are applied to derive the average physical condi-

[1] The National Aeronautics and Space Administration/Goddard Space Flight Center (NASA/GSFC) is responsible for the design, development, and operation of the *Cosmic Background Explorer* (*COBE*). Scientific guidance is provided by the *COBE* Science Working Group. GSFC is also responsible for the development of the analysis software and for the production of the mission data sets.

[2] Applied Research Corporation, Code 685.3, NASA/Goddard Space Flight Center, Greenbelt, MD 20771.
[3] Code 685, NASA/Goddard Space Flight Center, Greenbelt, MD 20771.
[4] Code 680, NASA/Goddard Space Flight Center, Greenbelt, MD 20771.
[5] General Sciences Corporation, Code 685.3, NASA/Goddard Space Flight Center, Greenbelt, MD 20771.

© American Astronomical Society • Provided by the NASA Astrophysics Data System

1994ApJ...428..638S

tions along each line of sight within the Galactic plane region and the large-scale physical conditions within the H_2, H I, and H II gas phases of the ISM. Because the DIRBE 140 and 240 μm observations primarily sample the ISM's large dust grain component, which attains an equilibrium temperature in the ambient radiation field, the results of our analysis can be combined with the results of the *IRAS* studies to arrive at a more complete interpretation of the large-scale FIR emission. At wavelengths of 140 and 240 μm, the Galaxy is transparent and is uncontaminated by emission from transiently heated dust particles.

In § 2, a summary of the data used in our analysis is presented. The average physical conditions along each line of sight in the Galactic plane region are derived in § 3. In § 4, the large-scale physical conditions within the H_2, H I, and H II gas phases of the ISM are derived. A brief summary of the results of the paper is presented in § 5.

2. DATA SETS AND PRELIMINARY DATA REDUCTION

A detailed description of the DIRBE instrument and *COBE* mission is given by Boggess et al. (1992). Galactic plane region maps at wavelengths of 60, 100, 140, and 240 μm are shown in Figure 1 (Plate 6). Preliminary comparisons of DIRBE and *IRAS* sky brightness measurements show that, aside from modest calibration differences in gain and zero point, the DIRBE and low-resolution *IRAS* 60 and 100 μm data are virtually identical (*COBE* DIRBE Explanatory Supplement: The Galactic Plane Maps 1993). The mean gain factors by which *IRAS* brightnesses must be multiplied to agree with DIRBE measurements are 0.87 and 0.72 at 60 and 100 μm, respectively. The 140 and 240 μm observations used in this paper are from data averaged over 10 months of cryogenic operation. Preliminary absolute calibration of the 140 and 240 μm bands is based on observations of Jupiter and has an estimated uncertainty of $\sim$10%. No attempt has been made to remove the zodiacal-light component from the observations. Throughout the paper, the uncertainties that are introduced into our analysis due to the presence of this component will be taken into account. Since our analysis is primarily restricted to the region $|b| < 1\overset{\circ}{.}25$, where the zodiacal component is everywhere estimated to be less than 15% of the observed 140 μm emission and less than 6% of the observed 240 μm emission, the presence of zodiacal emission will not lead to large uncertainties in our derived results.

The radio data used in this paper comprise the Galactic plane surveys of ^{12}CO from the Goddard Institute for Space Studies (Dame et al. 1987), the Berkeley/Hat Creek (Weaver & Williams 1973, 1974a, b), Maryland/Parkes (Kerr et al. 1986), and NRAO (Burton & Liszt 1983) Galactic plane surveys of neutral atomic hydrogen, and the Haynes, Caswell, & Simons (1978) Galactic plane survey of the 5 GHz radio continuum. The H I surveys provide nearly complete coverage of the entire Galactic plane region ($|b| < 10°$). The ^{12}CO surveys cover 94% of the region $0° < \ell < 360°$, $|b| < 5°$, and cover 68% of the entire Galactic plane region ($|b| < 10°$). The 5 GHz radio-continuum survey covers $\sim$90% of the region $280° < \ell < 40°$, $|b| < 1\overset{\circ}{.}5$.

Galactic plane region maps of the 140 μm, 240 μm, and 5 GHz radio-continuum emission and of the velocity-integrated ^{12}CO and H I emission at various angular resolutions were derived to facilitate comparison of the radio data with the DIRBE data. The velocity-integrated H I maps were derived by correcting the line profile along each line of sight for finite optical depth by assuming a uniform H I spin temperature of 140 K, and then integrating over the entire velocity range of the respective survey. Adopting other spin temperatures within 20 K of our assumed value changes the velocity-integrated H I intensities by less than a few percent. The velocity-integrated ^{12}CO maps were derived by integrating the data at a given longitude over the velocity interval where emission was detected in a velocity-longitude map of the Galactic plane region. The degradation of the FIR and radio data to lower angular resolution and the restriction of the velocity-integration range of the ^{12}CO data (Dame et al. 1987) enhances the signal-to-noise ratio in the resulting maps.

3. THE ISOTHERMAL DUST MODEL

3.1. *Analysis*

Maps of total H-atom column density, $N_{\rm H}$, at various angular resolutions were derived from the velocity-integrated ^{12}CO and H I emission maps using the relation $N_{\rm H_2} = XI_{^{12}\rm CO}$, where $I_{^{12}\rm CO}$ is the velocity-integrated ^{12}CO intensity, $N_{\rm H_2}$ is the molecular hydrogen column density, and $X = 2.0 \times 10^{20}$ molecules cm^{-2} K^{-1} km^{-1} s (Lebrun et al. 1983). Only pixels that satisfy at least one of the following criteria were included in the analysis: (1) The velocity-integrated ^{12}CO intensity is greater than 3 times the estimated rms noise level, $\sigma_{^{12}\rm CO}$; (2) $N_{\rm H\,I}$ is greater than $6X\sigma_{^{12}\rm CO}$. This leaves about 40% of the pixels in the maps of $N_{\rm H}$ unused, predominantly at $|b| > 5°$. The imposition of these criteria significantly reduced the errors in $N_{\rm H}$ that would have resulted from low signal-to-noise ratios in the velocity-integrated ^{12}CO maps. From the maps of the 140 and 240 μm emission and of $N_{\rm H}$, maps and longitude profiles of the dust temperature, T_d, the 240 μm optical depth, τ_{240}, the total FIR brightness, $I_{\rm FIR}$ (integrated over $\lambda > 40$ μm), the gas-to-dust mass ratio, G_d, and the total FIR luminosity per hydrogen mass, $L_{\rm IR}^{\rm H}$, were derived by assuming an isothermal dust distribution along each line of sight, a λ^{-2} dust emissivity law, and a dust mass absorption coefficient at 240 μm, κ_{240}, of 7.2 cm^2 g^{-1} (see Hauser et al. 1984 and Paper I for details of this type of analysis). The longitude profiles, shown in Figure 2, represent the mean properties over the $-0\overset{\circ}{.}75$ to $+0\overset{\circ}{.}75$ latitude interval, and the sampling in longitude is $0\overset{\circ}{.}5$.

The assumption of an isothermal dust distribution along each line of sight is clearly a simplification (Paper II; § 4, below). Since there exist warm and cold dust components along each line of sight, the derived values of dust temperature are biased toward the higher temperature components, resulting in underestimates of τ_{240}. However, as shown below, the derived values of T_d and τ_{240} are a significant improvement over the values of these quantities derived in Paper I using the *IRAS* 60 and 100 μm data. It is believed that the uncertainties in the derived values of $I_{\rm FIR}$ from the simple, single-temperature analysis are small (<20%). Based on the multi-temperature dust model derived in § 4 and on the long-wavelength behavior of the Galactic spectrum observed by FIRAS (Wright et al. 1991), the assumption of a single dust temperature along each line of sight results in an error of less than 10% in each of the derived values of $I_{\rm FIR}$. If one were to adopt a different emissivity index within the range $1.5 < n < 2.5$, 98% of the derived values of $I_{\rm FIR}$ would change by less than 15%. The derived values of $I_{\rm FIR}$ have been compared with $I'_{\rm FIR}$, the values of total FIR brightness derived in Paper I using the *IRAS* 60 and 100 μm data and assuming for each line of sight a single dust temperature with a λ^{-2} dust

© American Astronomical Society • Provided by the NASA Astrophysics Data System

1994ApJ...428..638S

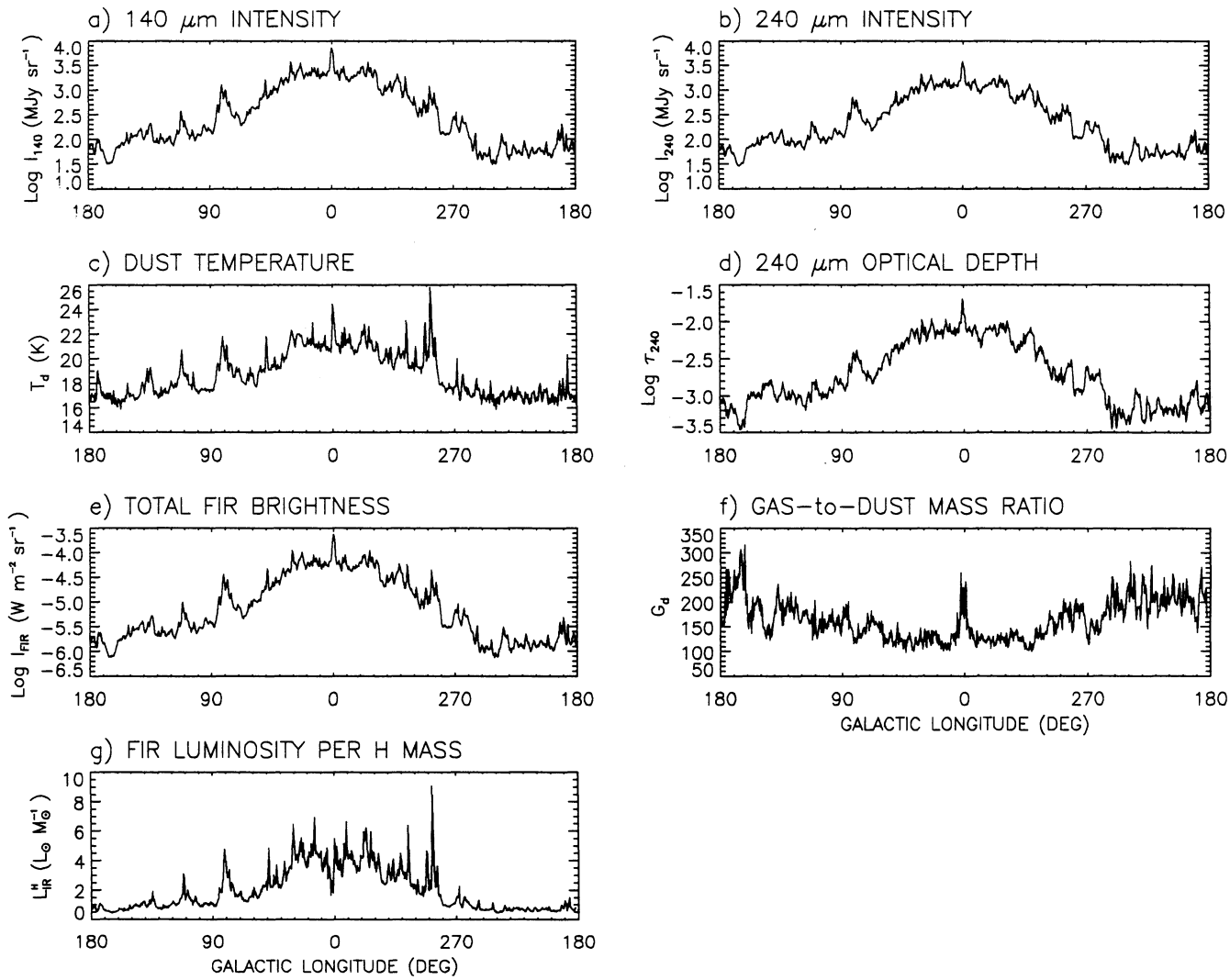

FIG. 2.—Longitude profiles of the Galactic large-scale FIR emission, averaged over the latitude region $|b| < 0.^\circ75$, and derived large-scale Galactic properties: (*a*) 140 μm emission; (*b*) 240 μm emission; (*c*) dust temperature; (*d*) 240 μm optical depth; (*e*) total FIR brightness; (*f*) gas-to-dust mass ratio; (*g*) FIR luminosity per H mass.

emissivity law. The quantity $I_{\rm FIR}/I'_{\rm FIR}$ has a mean value over the entire range of longitude of 1.26 and a standard deviation of $\sigma = 0.20$. While the mean ratio differs from unity in large part because of error in the *IRAS* bolometric correction due to the neglect of non-equilibrium emission and/or the calibration differences between the two sets of measurements, the modest dispersion indicates similar trends. A $\lambda^{-1.5}$ emissivity law would have raised the dust temperature and total FIR brightness by average fractions of 15% and 5%, respectively, and lowered the optical depth at 240 μm by an average fraction of 50%. However, these changes would not significantly affect the various trends in the derived quantities, which are the primary issue of this paper. The derived quantities depend on the 240-to-140 μm intensity ratio, R, approximately as R^α, where, for an emissivity index of $n = 2$, $\alpha = -0.54$, -1.35, and 1.8 for the dust temperature, total FIR brightness, and 240 μm optical depth, respectively.

3.2. *The Derived Quantities*

The longitude profiles in Figure 2 exhibit a general trend of decreasing dust temperature, optical depth, total FIR brightness, dust-to-gas mass ratio, and FIR luminosity per hydrogen mass from the inner ($270^\circ < \ell < 350^\circ$; $10^\circ < \ell < 90^\circ$) to the outer ($90^\circ < \ell < 270^\circ$) Galaxy, with the mean values of these derived quantities decreasing by factors of 1.2, 5, 15, 1.4, and 3, respectively (see Table 1). Since the statistical uncertainties are typically less than a few percent for the profiles of T_d, τ_{240}, and $I_{\rm FIR}$, and typically less than 10% for the profiles of G_d and $L^{\rm H}_{\rm IR}$, the general trend in each profile is highly significant. The mean values over all longitudes of T_d, τ_{240}, G_d, and $L^{\rm H}_{\rm IR}$ are 19 K, 0.003, 160, and 2 $L_\odot\ M_\odot^{-1}$, respectively. The derived values for τ_{240} show that, averaged over the $0.^\circ7$ DIRBE beam, the Galaxy is optically thin at 140 and 240 μm.

The longitudinal trend of T_d suggests that the dust temperature decreases significantly with increasing Galactocentric distance, D_G. To test this hypothesis, the latitude profile of the dust temperature at various longitudes was examined (see Fig. 3). The profiles show a general trend of decreasing dust temperature with increasing latitude for the inner Galaxy, and a reverse trend for the outer Galaxy. This behavior is also characteristic of a dust temperature profile that decreases with increasing D_G. Fitting an axisymmetric disk model to the lower

© American Astronomical Society • Provided by the NASA Astrophysics Data System

1994ApJ...428..638S

TABLE 1

DERIVED GALACTIC PROPERTIES

Quantity	Mean Values[a]		
	Inner Galaxy ($270° < \ell < 350°$; $10° < \ell < 90°$)	Outer Galaxy ($90° < \ell < 270°$)	Entire Galaxy
Dust temperature (K)	20 ± 1	17 ± 1	19 ± 1
240 μm optical depth	$(5.0 \pm 2.0) \times 10^{-3}$	$(9.5 \pm 3.0) \times 10^{-4}$	$(3.0 \pm 1.0) \times 10^{-3}$
Total FIR brightness (W m^{-2} sr^{-1})	$(3.7 \pm 0.3) \times 10^{-5}$	$(2.4 \pm 0.2) \times 10^{-6}$	$(2.0 \pm 0.2) \times 10^{-5}$
Gas-to-dust mass ratio	140 ± 50	190 ± 60	160 ± 60
FIR luminosity per H mass ($L_\odot/M_\odot$)	3.0 ± 0.3	0.9 ± 0.1	2.0 ± 0.2

NOTE.—A similar table based on analysis of *IRAS* 60 and 100 μm data can be found in Paper I (p. 107).

[a] Quoted error estimates are based on the 10% calibration uncertainty. See text for discussion of other sources of error.

envelopes of the intensity-longitude profiles, the radial behavior of the dust temperature can be described by an exponentially decreasing function in D_G, with a scale length of $\sim$21 kpc. In this axisymmetric disk, the dust temperature increases from a value of $T_d = 18.6$ K at the solar circle ($D_G = 8.5$ kpc) to values of 23 K at $D_G = 4$ kpc, and 28 K at the Galactic center.

The longitude profile of dust temperature derived here differs significantly from that derived from the *IRAS* 60 and 100 μm data under the same assumptions (Paper I). The latter was essentially constant with longitude, this behavior attributed to the contribution of small thermally fluctuating dust grains with radii $\lesssim$200 Å to the Galactic 60 μm emission. These small dust grains contribute negligibly to the 140 and 240 μm emission (Draine & Anderson 1985; Weiland et al. 1986; Désert et al. 1990) so that the currently derived temperature-longitude, temperature-latitude, and temperature–Galactocentric distance profiles are characteristic of large dust grains emitting at the equilibrium temperature. Therefore, the trends in these profiles, and the trend in the longitude profile of $L_{\rm IR}^{\rm H}$, suggest that the radiation field that heats the dust decreases with increasing Galactocentric distance. The derived values of T_d are in close agreement with those expected for dust heated by the Galaxy's ambient interstellar radiation field (ISRF; Cox, Krügel, & Mezger 1986), suggesting that the ISRF is the primary heating mechanism for most of the dust in the Galactic disk. From the currently derived temperature-longitude profile, a longitude profile of the expected 60-to-100 μm intensity ratio for dust grains radiating at the equilibrium temperature was derived. Stochastically heated dust grains do not contribute significantly to the 100 μm emission. Therefore, a comparison between the equilibrium 60-to-100 μm intensity ratios and those derived from the *IRAS* observations (Paper I) will yield the fractional contribution of the stochastically heated dust grains to the 60 μm *IRAS* band. It is found that the average values of this contribution are $\sim$40% and $\sim$60% in the inner and outer Galaxy, respectively.

Available evidence indicates that the derived constancy of the *IRAS* 60-to-100 μm intensity ratio with longitude (Paper I) is not a consequence of the nonlinear responsivities of the *IRAS* 60 and 100 μm detectors. Dust temperatures derived using the zodiacal-corrected *IRAS* 100 μm data (Paper I) and the DIRBE 140 μm data agree to within a few percent with the derived temperatures in Figure 2*c*, suggesting that *IRAS* 100 μm response nonlinearities for $|b| < 0\overset{\circ}{.}75$ do not cause serious errors in the longitudinal brightness variation.

The mean value of G_d is 160, a value consistent within the uncertainties with the canonical value of $\sim$100, considering the simplified assumption of an isothermal dust distribution along each line of sight, the choice of a specific emissivity index, and the factor of 2 or more uncertainty in the adopted values of X (Combes 1991) and κ_{240} (Draine 1990). The longitudinal

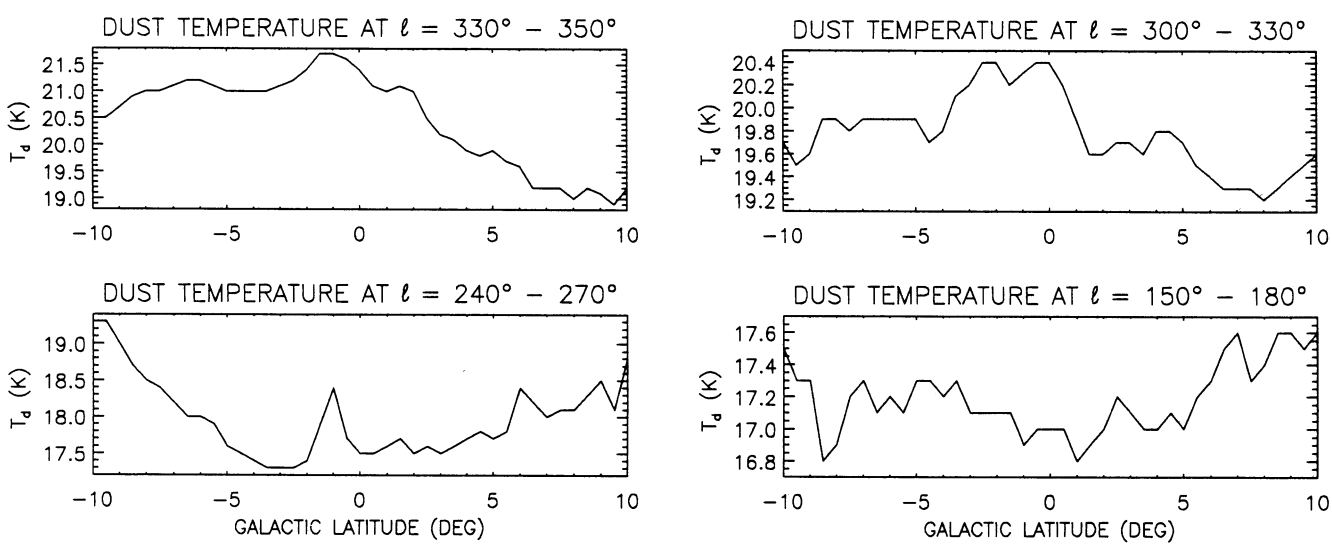

FIG. 3.—Latitude distribution of dust temperature. The longitude bins were chosen to minimize the contribution from zodiacal light to the emission in the DIRBE 140 and 240 μm bands.

© American Astronomical Society • Provided by the NASA Astrophysics Data System

1994ApJ...428..638S

trend of G_d is consistent with the observed increase in metallicity toward the Galactic center, as expected if the abundance of the dust traces that of the heavy elements (Panagia & Tosi 1981; Shaver et al. 1983; Wannier 1989). It is important to note that the profiles of G_d and $L_{\rm IR}^{\rm H}$ were derived using a constant value of X for the entire Galactic plane region. There is, however, evidence for an increase in the value of X with increasing Galactocentric distance (Sodroski 1991). Based on this suggested behavior of X with Galactocentric distance, its longitudinal dependence was derived. Using this longitudinally varying X, it is found that the derived gradients in G_d and $L_{\rm IR}^{\rm H}$ increase by about 20%.

It should be noted, however, that G_d is strongly temperature dependent, so that its longitudinal behavior may be significantly different in a more realistic model in which the dust will have a distribution of temperatures along each line of sight. For example, a very cold dust component with a temperature of less than 10 K and a mass equal to that of a warm dust component at a temperature of 17 K will contribute less than 10% of the flux in the DIRBE 140 and 240 μm bands. Therefore, most of the cold dust component would remain undetected by DIRBE. In their analysis of the FIRAS Galactic spectrum, Wright et al. (1991) could not rule out excess long-wavelength emission over that expected for a single-temperature dust model with a λ^{-2} emissivity law. They concluded that the allowed excess emission could arise from a dust component composed of spherical grains radiating at an equilibrium temperature of $\sim$5 K and having a mass greater than 80% of the total dust mass. Needles or fractal dust grains (Wright 1987; Bazell & Dwek 1990) are significantly more efficient emitters at long wavelengths than spherical dust grains. Therefore, if a population of such grains exists, it could give rise to the allowed excess emission and have a mass that is less than a few percent of the total dust mass (Wright 1993).

Within 2° of longitude of the Galactic center, G_d reverses its general trend and increases by a factor of $\sim$2–3 toward the Galactic center. This increase in G_d is in contrast to the expected decrease by a factor of $\sim$2–3 in G_d assuming (Mezger et al. 1986) that the dust-to-gas mass ratio traces the metallicity, which is a factor of $\sim$2–3 higher in the Galactic center region (Galactocentric distance $<$300 pc) than in the inner Galactic disk (Wannier 1989; Cox & Laureijs 1989). One possible explanation for this discrepancy is that the value of X is a factor of $\sim$4–9 lower in the Galactic center region than in the Galactic disk and, therefore, that the adopted value of X overestimates the H_2 column density along lines of sight near the Galactic center by the same factor. That the ratio of H_2 column density to ^{12}CO intensity in the Galactic center region is more than a factor of 6 lower than its nominal Galactic value has been suggested by Blitz et al. (1985) as one possible interpretation of the relative deficiency of high-energy (300 MeV to 5 GeV) γ-ray emission from the Galactic center region compared to the disk.

4. THE LARGE-SCALE PHYSICAL CONDITIONS OF THE DUST IN THE VARIOUS GAS PHASES OF THE ISM

4.1. *Linear Decomposition of the 140 and 240 μm Data*

A visual comparison of Figure 1 with ^{12}CO, H I, and 5 GHz radio-continuum maps shows that in general the Galactic large-scale FIR emission is well correlated with the emission from the H_2, H I, and H II gas phases of the ISM (Paper I). In Sodroski et al. (1986) and Paper II, a mathematical inversion technique was presented which, by taking into account both the small-scale and large-scale structure in the FIR and radio maps, allowed us to accurately decompose the Galactic large-scale 60 and 100 μm emission observed by *IRAS* into its various gas phase components. In this section, the decomposition method is applied to the full-resolution 140 and 240 μm data within the region $300° < \ell < 40°, |b| < 1°.25$.

In this approach, the observed FIR intensity at a given wavelength, λ, along each line of sight (ℓ, b), is given by

$$I_{\rm FIR}(\ell, b, \lambda) = \epsilon_{\rm H_2}(\ell, b, \lambda)N_{\rm H_2}(\ell, b) + \epsilon_{\rm H\,I}(\ell, b, \lambda)N_{\rm H\,I}(\ell, b) + \epsilon_{\rm H\,II}(\ell, b, \lambda)N_{\rm H\,II}(\ell, b)\,, \quad (1)$$

where the ϵs represent the FIR emissivities per H atom in the respective gas phases. The ^{12}CO, H I, and 5 GHz radio-continuum surveys are used to derive H-atom column density maps for the three gas phases, at $\sim$0°.7 resolution. The FIR and radio maps are divided into subregions of size $\Delta\ell = 10°$ and $\Delta b = 2°.5$ centered on the Galactic plane, with each subregion containing 105 lines of sight. Assuming that within each subregion the emissivities are constant, equation (1) becomes an overdetermined system of 105 equations which can be solved for the three unknown emissivities of the subregion. From the resulting emissivities and H-atom column density maps, longitude profiles of the large-scale physical conditions within each gas phase of the ISM are derived.

Figure 4 shows the observed and calculated 140 and 240 μm intensities at $b = 0°$ for the entire range of longitude over which the linear decomposition method was applied. Figure 5 is a comparison of the observed and calculated latitude distributions for one of the subregions and also shows the respective contributions from each gas phase component. The results of the analysis of the 60 and 100 μm *IRAS* data in Paper II are also shown in Figure 5. The relative contribution to the FIR intensity from the molecular component increases with increasing wavelength, whereas that from the ionized component decreases with increasing wavelength, consistent with the generally accepted view that dust associated with ionized gas has a higher equilibrium temperature than dust associated with molecular gas.

4.2. *Derived Physical Conditions*

4.2.1. *Longitude Profiles of Dust Temperature and FIR Luminosity per Hydrogen Mass*

Figure 6 shows longitude profiles of the derived dust temperature and FIR luminosity per hydrogen mass for the H I and H_2 gas phases of the ISM, and Table 2 summarizes the derived Galactic properties of the dust within each of the three gas phases. A similar table can be found in Paper II (Table 3). A morphological comparison of the FIR and radio emission in Figure 7 shows that the FIR emission from the outer Galaxy originates largely from dust associated with the H I gas phase (see also Paper I). Since it is also true that most ($>$90%) of the mass in the outer Galaxy is in the form of neutral atomic hydrogen (Mezger 1978; Henderson, Jackson, & Kerr 1982; Bloemen 1985), it follows that the outer Galaxy values for T_d and $L_{\rm IR}^{\rm H}$ derived with our single-temperature analysis (§ 3) are characteristic of dust associated with the H I gas. The dust temperature and FIR luminosity per hydrogen mass for the H I component increase systematically with longitude toward the Galactic center (Fig. 6), and the mean values of these quantities increase from the outer to the inner Galaxy by factors of 1.25 and 4, respectively (Table 2). This behavior is consistent with

© American Astronomical Society • Provided by the NASA Astrophysics Data System

1994ApJ...428..638S

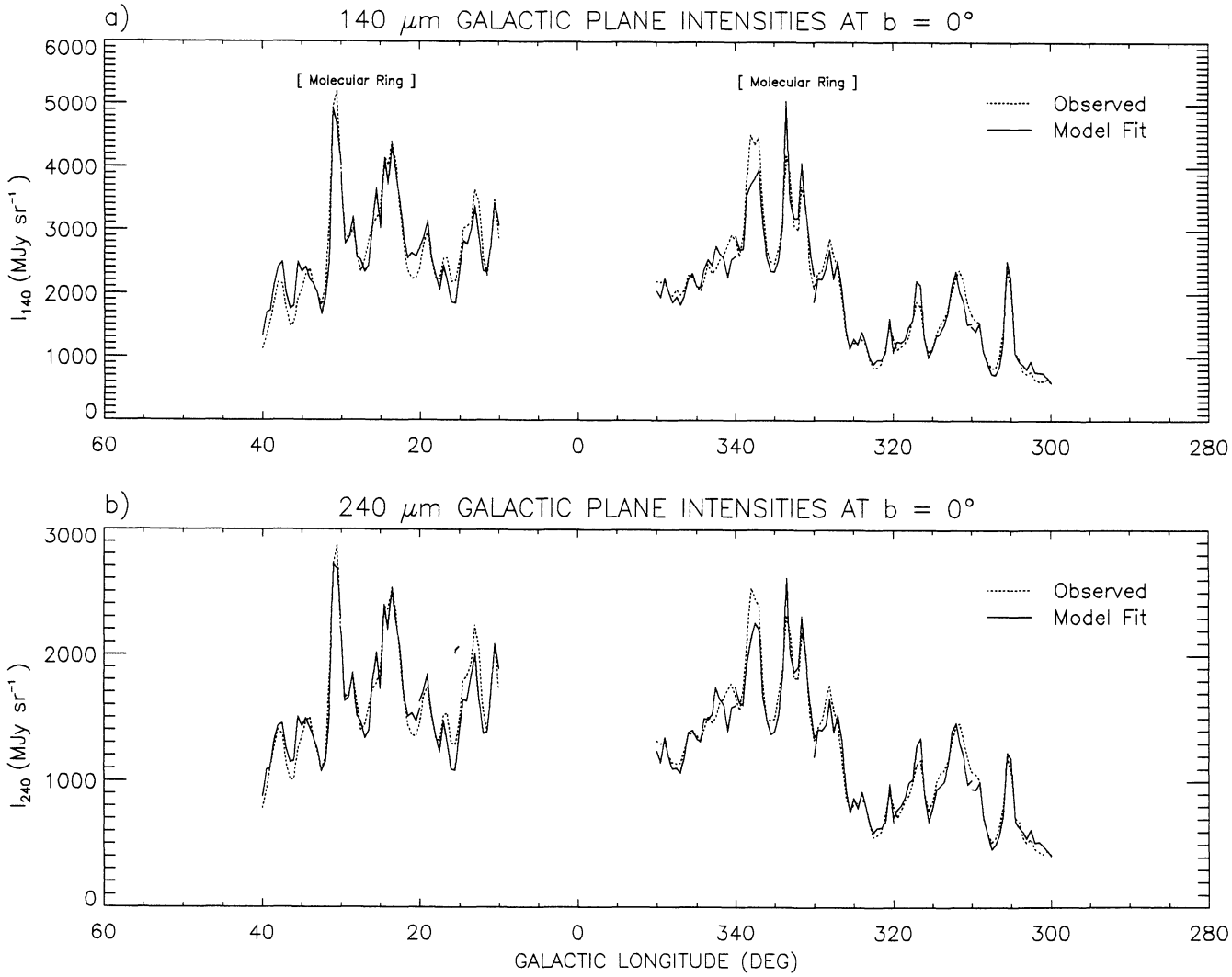

FIG. 4.—(*a*) Longitude profile of the observed 140 μm Galactic plane emission, averaged over latitude interval $|b| < 0\overset{\circ}{.}75$ (*dotted line*), and fit to observed profile from decomposition algorithm (*solid line*). (*b*) Same as (*a*), for 240 μm Galactic plane emission.

an increase by a factor of ~ 4 in the ISRF (Mathis, Mezger, & Panagia 1983; Cox et al. 1986), which is the primary dust heating source for the diffuse H I gas.

The most significant difference emerging from the comparison of the current results with those from *IRAS* (see Paper II) is the longitudinal trend in the temperature of the dust associated with the H I gas. The *IRAS* results exhibit a flat temperature profile at ~ 24 K, whereas the DIRBE results show a distinct drop in temperature, from ~ 22 K at $\ell = 10°$–$30°$, 330°–350°, to ~ 20 K at $\ell = 30°$–$40°$, 300°–330°, to 17 K in the outer Galaxy. The constancy of dust temperature inferred from the *IRAS* data was attributed to the contribution of stochastically heated dust particles to the emission in the 60 μm *IRAS* band. Uncontaminated by that contribution, the 140-to-240 μm emission ratio reflects the "true" equilibrium dust temperatures in the various gas phases of the ISM.

4.2.2. *Mean Dust Temperatures and Gas-to-Dust Mass Ratios*

The mean dust temperatures for the molecular and ionized gas phases (Table 2) are very similar to the corresponding mean dust temperatures derived in Paper II. The mean inner Galaxy gas-to-dust mass ratios for all three gas phases are consistent, within the uncertainties, with the local canonical value of ~ 100.

4.2.3. *Global Energetics*

From the derived values of the mean FIR luminosity per hydrogen mass for each of the three gas phases and from previous estimates of the total mass of each gas phase (Mezger 1978; Henderson et al. 1982; Dame 1983; Bloemen 1985),[6] the total FIR luminosity for each gas phase is derived. It is found that the total FIR luminosity ($\lambda > 40$ μm) of the Galactic disk is $\sim 1.1 \times 10^{10}$ $L_\odot$, with 70%, 20%, and 10% from dust associated with the neutral atomic hydrogen phase, the molecular phase, and the extended low-density ionized phase, respectively. These results are in close agreement with the results of the *IRAS* analyses of the Galactic plane (Sodroski et al. 1986; Paper I; Paper II; Bloemen et al. 1990; and references therein).

[6] The adopted gas mass estimates were originally derived using a solar distance to the Galactic center of $R_\odot = 10$ kpc. Based on the recommended value of $R_\odot = 8.5$ kpc by IAU Commission 33 (see Kerr & Lynden-Bell 1986), the original gas mass estimates have been reduced by a factor of ~ 0.7.

© American Astronomical Society • Provided by the NASA Astrophysics Data System

1994ApJ...428..638S

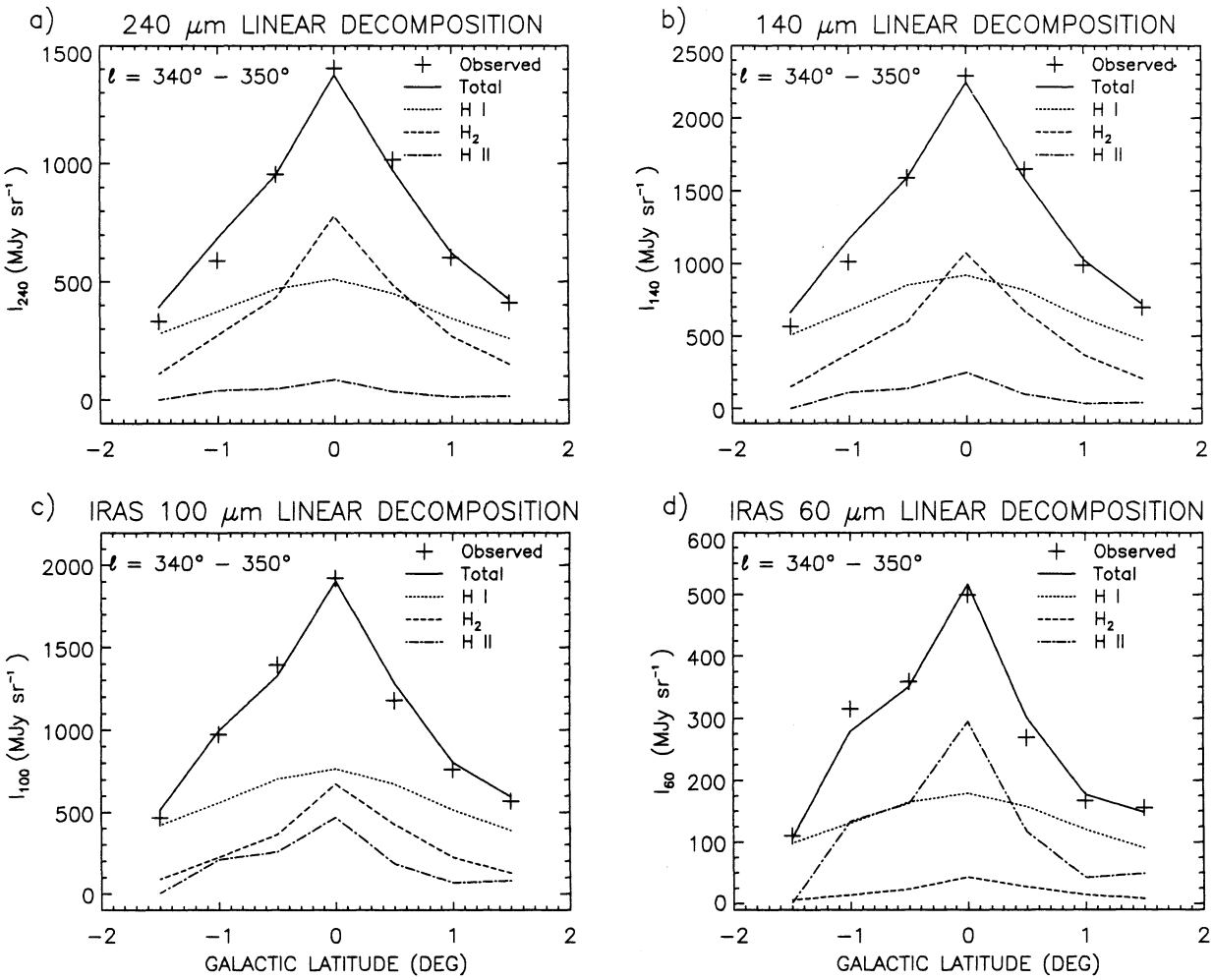

FIG. 5.—(*a*) Sample of observed (*plus signs*) and calculated (*solid line*) latitude distributions of 240 μm emission from the linear decomposition. Also shown are the respective contributions to the calculated intensity-latitude profile from dust associated with H_2 (*dashed line*), H I (*dotted line*), and H II (*dot-dashed line*) components. (*b*) Same as (*a*), for 140 μm emission. (*c*) Same as (*a*), for 100 μm emission (from Paper II). (*d*) Same as (*a*), for 60 μm emission (from Paper II).

It has been estimated (Paper II) that mid-infrared ($\lambda < 40$ μm) emission from small, stochastically heated grains constitutes about 30%–50% of the total Galactic infrared (IR) luminosity. Therefore, it is estimated that the total IR luminosity of the Galactic disk is ~ 1.6–2.2×10^{10} $L_\odot$, which is in agreement with the estimate for the total Galactic IR luminosity derived by Wright et al. (1991) using FIRAS measurements (100 μm $< \lambda <$ 1000 μm) and a bolometric correction.

4.2.4. *Relevance of the Warm Ionized Medium*

The analysis presented in this section does not attempt to fit a component for the warm ionized medium (WIM; McKee & Ostriker 1977). The WIM, distinguishable from the extended low-density ionized (H II) gas phase by its lower density (~ 0.1 cm^{-3}) and larger scale height (~ 900 pc; Reynolds 1991), is not traced by the 5 GHz radio-continuum survey of Haynes et al.

TABLE 2

GLOBAL GALACTIC PROPERTIES WITHIN THE GAS PHASES OF THE ISM

Gas Phase	Dust Temperature (K)	Gas-to-Dust Mass Ratio	FIR Luminosity per H Mass ($L_\odot M_\odot^{-1}$)	Total Mass[a] ($M_\odot$)	Total FIR Luminosity ($10^9 L_\odot$)
H_2 (inner Galaxy)	19.0 ± 1.0	115 ± 20	2.7 ± 0.1	0.7×10^9 [b]	1.9 ± 0.1
H I (inner Galaxy)	21.0 ± 1.0	140 ± 20	3.8 ± 0.4	...	...
H I (outer Galaxy)	17.0 ± 1.0	190 ± 60	0.9 ± 0.1	...	...
H I (entire Galaxy)	18.5 ± 1.0	170 ± 30	2.3 ± 0.2	3.5×10^9 [c]	8.1 ± 1.0
H II (inner Galaxy)	29.0 ± 3.0	100 ± 40	34.0 ± 10.0	2.7×10^7 [d]	0.9 ± 0.3

NOTE.—A similar table based on analysis of *IRAS* 60 and 100 μm data can be found in Paper II (p. 776).

[a] Corrected for $R_\odot = 8.5$ kpc.

[b] Dame 1983; Bloemen 1985.

[c] Henderson et al. 1982.

[d] Mezger 1978.

© American Astronomical Society • Provided by the NASA Astrophysics Data System

1994ApJ...428..638S

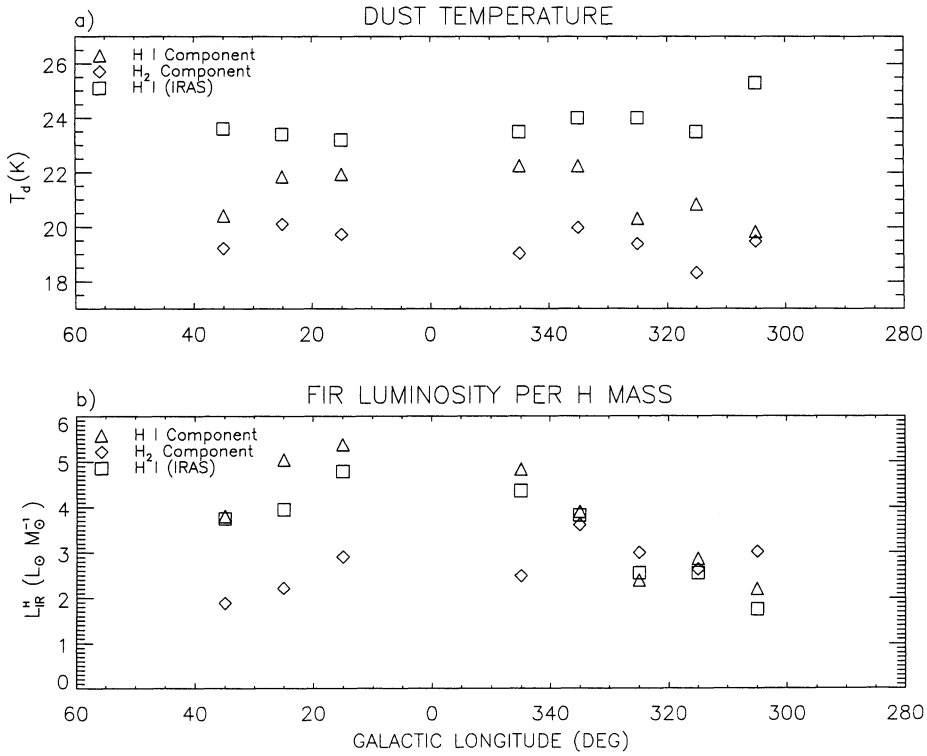

FIG. 6.—(*a*) Derived dust temperature and (*b*) derived FIR luminosity per H mass profiles for the H I (*triangle*) and H_2 (*diamond*) gas phases from the linear decomposition of the DIRBE 140 and 240 μm data. Also shown are the results for the H I gas phase (*square*) from the linear decomposition of the *IRAS* 60 and 100 μm data (from Paper II). The statistical uncertainties of the FIR luminosity per H mass for the H I gas phase are $\sim$20%. All of the other derived quantities have statistical uncertainties of $\sim$10%.

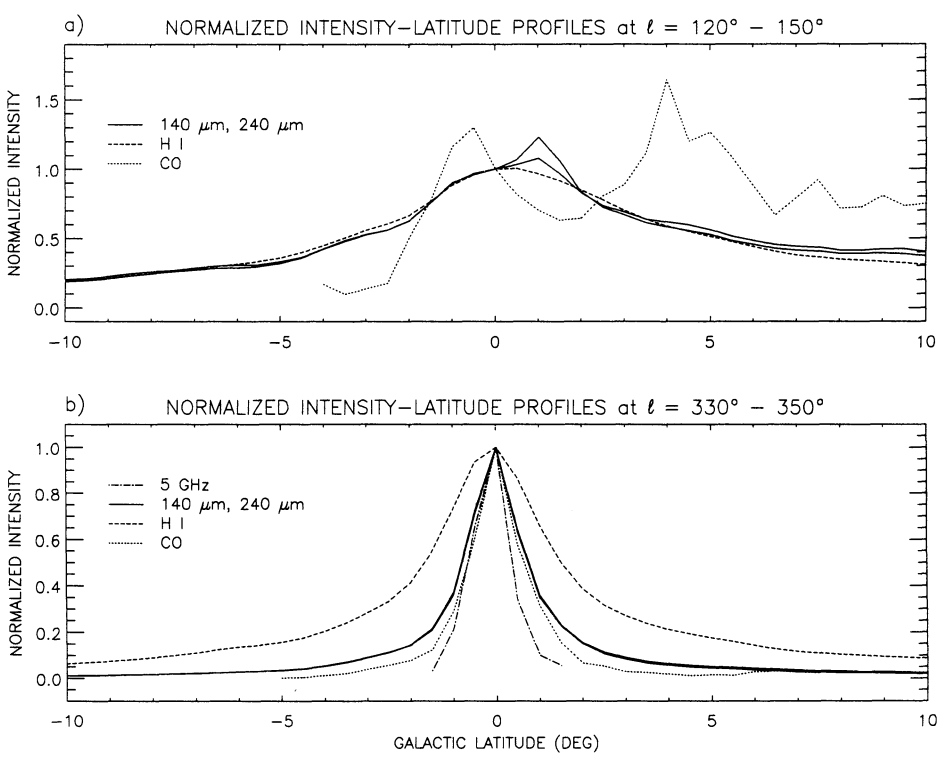

FIG. 7.—Comparison of the latitude distributions of the 140 and 240 μm, ^{12}CO, H I, and 5 GHz radio-continuum emission for representative regions in the (*a*) outer and (*b*) inner Galaxy. Each of the profiles has been normalized to its intensity at $b = 0°$ and has an angular resolution in latitude of $\sim 0\overset{\circ}{.}7$. In the outer Galaxy, the latitude distributions of the 140 and 240 μm emission are very similar to the latitude distribution of the H I emission, but are significantly different from the latitude distribution of the ^{12}CO emission, suggesting that the FIR emission from the outer Galaxy originates largely from dust associated with the H I gas. In the inner Galaxy, the latitude distributions of the 140 and 240 μm emission are slightly broader than the latitude distributions of the ^{12}CO and 5 GHz radio-continuum emission, yet considerably narrower than that of the H I emission, suggesting that a significant fraction of the FIR emission in the inner Galaxy originates from dust associated with each of the three gas phase components.

© American Astronomical Society • Provided by the NASA Astrophysics Data System

1994ApJ...428..638S

due to the WIM's low emission measure. In their analysis of the FIRAS spectrum of the Galactic plane region, Wright et al. (1991) suggested that a significant fraction ($\sim$25%) of the FIR luminosity that in Paper II is attributed to dust associated with the H I component actually arises from dust within the WIM. The estimate of Wright et al. (1991) is based in part on the derived fraction of FIR flux in the 205 μm line of N II, on an adopted value of IRE (i.e., the FIR-to-Lyα luminosity ratio) for the WIM equal to that derived in Paper II for extended low-density H II regions, and on the H II region models of Rubin (1985).

The relevance of the WIM to studies of the Galactic large-scale FIR emission has also been addressed by Boulanger & Désert (1992), who have estimated that dust within this gas phase component is expected to give rise to $\sim$25% of the IR emission at high ($|b| > 10°$) Galactic latitude, based on estimates of the mass of this component in the solar vicinity and on an adopted dust-to-gas mass ratio for this component equal to that for the Galaxy's neutral gas. However, Boulanger & Désert find no evidence for residual 100 μm emission in their correlation of latitude profiles of 100 μm and velocity-integrated H I emission from high-latitude cirrus. Although there is some controversy concerning the magnitude of FIR emission of the WIM, the relative contribution of the WIM in our fits at low Galactic latitude should be much less than 25%.

5. SUMMARY

In this paper, the DIRBE 140 and 240 μm observations of the Galaxy were used to derive the large-scale properties of the dust within $|b| < 10°$, first, by assuming an isothermal dust model along each line of sight and, second, by decomposing the 140 and 240 μm emission into its constituent components associated with the H_2, H I, and the H II phases of the ISM. The results of our analysis can be briefly summarized as follows:

1. The Galactic FIR luminosity is 1.1×10^{10} $L_\odot$. About 60%–75% of this energy arises from cold (17–22 K) dust associated with diffuse H I clouds, and 15%–30% arises from $\sim$19 K dust residing in molecular clouds. Dust within extended low-density ($n_e \sim 10$–100 cm^{-3}) H II regions radiates at $\sim$29 K, but contributes less than $\sim$10% to the total FIR luminosity of the Galaxy.

2. The derived results are consistent with models in which the contribution from small (5 Å $\lesssim$ radius $\lesssim$200 Å) transiently heated dust particles to the Galactic emission at wavelengths greater than 140 μm is negligible. Therefore, the dust temperatures derived using the DIRBE 140 and 240 μm observations are characteristic of the equilibrium temperatures for large dust grains. The longitudinal and latitudinal trends in dust temperature suggest a general decrease in the ISRF with increasing Galactocentric distance.

3. The general longitudinal trend of an increasing dust-to-gas mass ratio toward the Galactic center is reversed in the inner 4° region. One possible explanation for this result is that the ratio of H_2 column density to ^{12}CO intensity in the Galactic center region is significantly lower than its mean Galactic value.

The authors gratefully acknowledge the efforts of the DIRBE data processing and validation teams in producing the high-quality data sets used in this investigation. We also thank J. Mather, N. Wright, and the rest of the *COBE* Science Working Group for helpful comments on this manuscript. We thank H. Liszt and W. B. Burton for providing us with the NRAO Galactic center H I survey data and T. Dame and P. Thaddeus for providing us with the Goddard-Columbia CO survey data.

REFERENCES

Bazell, D., & Dwek, E. 1990, ApJ, 360, 142
Blitz, L., Bloemen, J. B. G. M., Hermsen, W., & Bania, T. M. 1985, A&A, 143, 267
Bloemen, J. B. G. M. 1985, Ph.D. thesis, Sterrewacht Leiden
Bloemen, J. B. G. M., Deul, E. R., & Thaddeus, P. 1990, A&A, 233, 437
Boggess, N., et al. 1982, ApJ, 397, 420
Boulanger, F., & Désert, F. X. 1992, in The Infrared and Submillimetre Sky after *COBE*, ed. M. Signore et al. (Dordrecht: Kluwer), 263
Burton, W. B., & Liszt, H. S. 1983, A&AS, 52, 63
COBE DIRBE Explanatory Supplement: The Galactic Plane Maps. 1993, in directory: COBE/INITIAL_PRODUCTS/DIRBE/DOC (version 19 July 1993). Available from NSSDC at internet address: nssdca.gsfc.nasa.gov
Combes, F. 1991, ARA&A, 29, 195
Cox, P., Krügel, E., & Mezger, P. G. 1986, A&A, 155, 380
Cox, P., & Laureijs, R. 1989, in IAU Symp. 136, The Center of the Galaxy, ed. M. Morris (Dordrecht: Kluwer), 121
Cox, P., & Mezger, P. G. 1989, Astron. Astrophys. Rev., 1, 49
Dame, T. M. 1983, Ph.D. thesis, Columbia Univ.
Dame, T. M., et al. 1987, ApJ, 322, 706
Désert, F. X., Boulanger, F., & Puget, J. L. 1990, A&A, 237, 215
Draine, B. T. 1990, in The Interstellar Medium in Galaxies, ed. H. A. Thronson, Jr., & J. M. Shull (Dordrecht: Kluwer), 483
Draine, B. T., & Anderson, N. 1985, ApJ, 292, 494
Hauser, M. G., et al. 1984, ApJ, 285, 74
Haynes, R. F., Caswell, J. L., & Simons, L. V. S. 1978, Australian J. Phys., Astrophys. Suppl., 45, 1
Henderson, A. P., Jackson, P. D., & Kerr, F. J. 1982, ApJ, 263, 116
Hoffmann, W. F., & Frederick, C. L. 1969, ApJ, 155, L9
Kerr, F. J., Bowers, P. F., Jackson, P. D., & Kerr, M. 1986, A&AS, 66, 373
Kerr, F. J., & Lynden-Bell, D. 1986, MNRAS, 221, 1023
Lebrun, F., et al. 1983, ApJ, 274, 231
Mathis, J. S., Mezger, P. G., & Panagia, N. 1983, A&A, 128, 212
McKee, C. F., & Ostriker, J. P. 1977, ApJ, 218, 148
Mezger, P. G. 1978, A&A, 70, 565
Mezger, P. G., Chini, R., Kreysa, E., & Gemund, H. P. 1986, A&A, 160, 324
Neugebauer, G., et al. 1984, ApJ, 278, L1
Panagia, N., & Tosi, M. 1981, A&A, 96, 306
Reynolds, R. J. 1991, in IAU Symp. 144, The Interstellar Disk-Halo Connection in Galaxies, ed. H. Bloemen (Dordrecht: Kluwer), 67
Rubin, R. H. 1985, ApJS, 57, 349
Shaver, P. A., McGee, R. X., Newton, L. M., Danks, A. C., & Pottasch, S. R. 1983, MNRAS, 204, 53
Sodroski, T. J. 1991, ApJ, 366, 95
Sodroski, T. J., Dwek, E., Hauser, M. G., & Kerr, F. J. 1986, in Proc. Conf. Star Formation in Galaxies, ed. C. J. Persson (Washington, DC: GPO), 99
———. 1987, ApJ, 322, 101 (Paper I)
———. 1989, ApJ, 336, 762 (Paper II)
Wannier, P. G. 1989, in IAU Symp. 136, The Center of the Galaxy, ed. M. Morris (Dordrecht: Kluwer), 107
Weaver, H., & Williams, D. R. W. 1973, A&AS, 8, 1
———. 1974a, A&AS, 17, 1
———. 1974b, A&AS, 17, 251
Weiland, J. L., Blitz, L., Dwek, E., Hauser, M. G., Magnani, L., & Rickard, L. J. 1986, ApJ, 306, L101
Wright, E. L. 1987, ApJ, 320, 818
———. 1993, in Back to the Galaxy, ed. F. Verter & S. Holt (AIP Conf. Proc. 278), 193
Wright, E. L., et al. 1991, ApJ, 381, 200

© American Astronomical Society • Provided by the NASA Astrophysics Data System

1994ApJ...428..638S

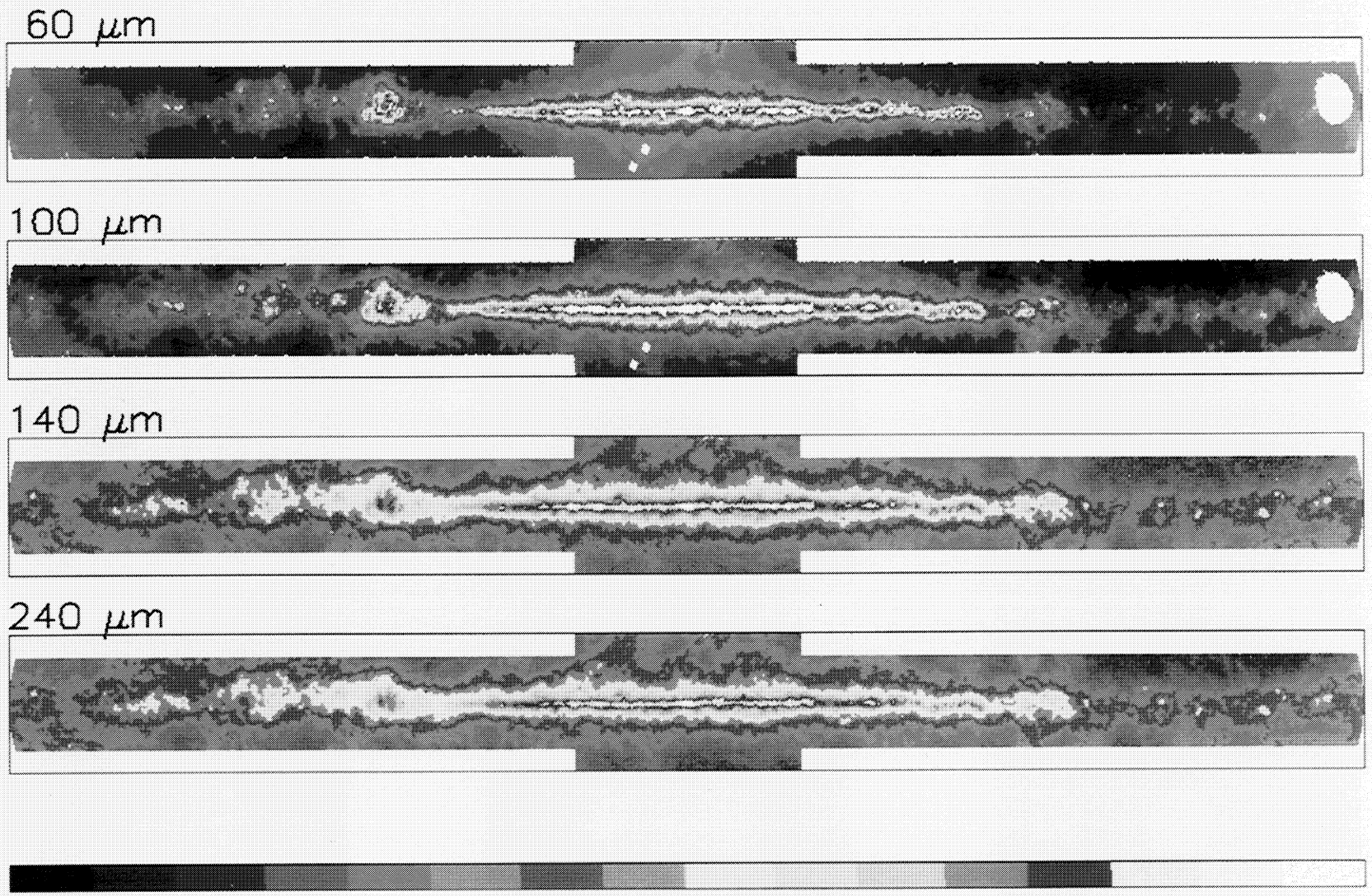

FIG. 1.—DIRBE images of the Galactic plane region at wavelengths of 60, 100, 140, and 240 μm. Each image is a Mollweide projection in Galactic coordinates with the Galactic center at the center of the image, and extends from $b = -10°$ to $10°$ for $30° < \ell < 330°$, and $b = -15°$ to $15°$ within 30° of longitude of the Galactic center. The 60 and 100 μm images were derived by interpolating the observations to a solar elongation angle of 90°. The 140 and 240 μm images were derived from data averaged over the entire 10 months of cryogenic operation. Emission from interplanetary dust appears at 60 μm as a broad band passing approximately through the Galactic center and anticenter. The three blanked regions in the 60 and 100 μm images are due to the exclusion of data near the planets Jupiter (*right*), Uranus (*center*), and Neptune (*center*). Each image is on a logarithmic scale over the intervals $\log_{10}(I[\mathrm{MJy\ sr^{-1}}]) = [0.8, 3.0]$ (60 μm); [0.8, 3.4] (100 μm); [0.4, 4.0] (140 μm); [0.4, 3.8] (240 μm).

SODROSKI et al. (see 428, 639)

PLATE 6

© American Astronomical Society • Provided by the NASA Astrophysics Data System